A unifying approach to kinetic structures composed by bar or plate 4R-linkages

A unifying approach to kinetic structures composed by bar or plate $4R$-linkages.

Valentina Beatini[a,*], Marcelo A. Dias[b]

[a] *Aarhus University, Dept. of Engineering, Aarhus, Denmark*
[b] *The University of Edinburgh, School of Engineering, Edinburgh, United Kingdom*

Abstract

This study deals with modular assemblies of 4R-linkages, whether spherical or planar, with the aim to highlight the underlying shared principles and contribute to posing the base for a grammar of modular kinetic assemblies. The two types of mechanisms are widely employed in applied research due to their simplicity combined with large morphological potentialities. However, since their application fields tend to differ, there is a lack of shared theory. In this paper, a unifying kinematic model of the single linkage, based on the Grashof's criterion, has been set and extended to linear assemblies. Focus has been made on fully rotatable assemblies and their applicability to approximate spatial open curves. The proposed method, relying on kinematics, is suitable for further expansion. To broaden the applicability of these concepts, it is noticed from the mechanical response of different types of configurations, that energetically optimal pathways may be designed.

Keywords: Foldable plate structures, Deployable structures, Modular $4R$-linkages, Kinetic structures, Origami, Scissors mechanisms.

1. Introduction

After the pioneering work of the architect Pérez Piñero [1], a rich body of works have been produced on the morphological possibilities of planar $4R$ linkages (linkages composed of 4 bars and 4 revolute joints), both experimental and theoretical investigations [2, 3]. The typical application ranges in size

*Corresponding author
Email address: valentina.beatini@cae.au.dk (Valentina Beatini)

from a few centimetres to metres and the fields of interests are within machinery (lifting equipment), furniture (chairs, extendable mirrors, etc), architecture (temporary pavilions), and deployable structures, such as roofs, bridges as well as booms and rings for space applications [3, 4, 5]. The implementation of such applications rely on structural and fabrication characteristics of linkages. Since links are designed as bars, the need for mechanical joints has hindered small-scale applications. In contrast, the structural assessment of rigid $2D$ pin-joined bars is relatively reliable.

Starting with the rediscovery of an ancient origami folding technique [6], modular spherical $4R$ linkages emerged as a research field within computational origami and have been extended to a wider range of possible applications; such as furniture design, temporary architectural pavilions and space applications. The underlying kinematic knowledge and the morphological possibilities explored by many of these applications can be traced in the OSME conference series [7, 8]. Since spherical linkages are continuous plate structures, their structural performances may be tuned to fit a diverse usages. In the past few years, the proposed applications have reached stiff architectural facade components, highly deformable biomedical applications, or shock-absorbing devices [9]. Finally, certain spherical linkages, "strict" origami identified in Section 2 can be manufactured with compliant joints, allowing micro- and nano-scale robotic fabrication technologies [10] to be investigated mainly to pursue self-folding systems [11].

As the definitions may suggest, there are analogies between the two types of linkages. In Chiang's contributions to the knowledge of spherical mechanisms [12, 13], the analogies between planar and spherical $4R$ linkages was introduced and extended to the Grashof's rotability theorem [14]. The latter topic has been further discussed in [15]. Interestingly, however, these connections have stayed mostly unexplored. This study extends this comparison between planar and spherical linkages to their assemblies.

The approach does not focus merely on the mathematical formulation for the rotatability of assemblies, as these have been expressed in the groundbreaking works of Escrig [16] and Tachi [17] for respectively planar and spherical mechanisms. However, these studies leave to the designer's understanding, through a time-consuming process of trial and error, which geometries can be parametrised and, among them, which can be implemented into fully rotatable modular linkages. On the other hand, much of applied research aim at reproducing target geometries with no interest in underlying the kinematic constraints and defining the related range of possible variations. This is the

case when the mechanism is used to solve a contingent problem external to the mechanism itself, such as the vertical movement of loads in scissor-based construction lifting equipment. More generally, when a new application is hypothesised, several functional, structural and aesthetic factors affect the design, which does not allow one aspect to be fully explored independently. This is typical of the many architectural applications, such as the bar linkages embedded in the designs of Santiago Calatrava [18], whose design process was part of a larger design involving the unique building, or non-repeatable prototype at hand.

The proposed method, relating the kinematics of the linkage with the assembly mode, overcomes the risk of partial results. Bridging the knowledge in planar and spherical kinematics, the method has allowed the development of a novel algorithm for generating planar linkages whose joints stay parallel when assembled along spatial curves. In the following Section, the kinematic model shared by the two types of linkages is developed, along with the assembly constraints. For consistency, the energy graphs of the planar and spherical linkages are contrasted. In Section 3, algorithms are described to obtain fully rotatable linkages given a prescribed set of points organised in space along an open curve. As detailed in the Section, the algorithms are based on assembling fully rotatable linkages discussed in Section 2.1, and such they refer again to the kinematic rules expressed in Section 2.3. This approach, already employed by those working on spherical linkages, differs from the typical one developed within scissor linkages [19] because the focus is normally on the proportion of the length of the links shared by adjacent linkages, an approach where the kinematic rules may appear less evident. Finally, a summary of the results and a discussion on the presented model's possible extension is provided in the conclusions.

2. The kinematic models

2.1. Kinematics of 4R-linkages

4R-linkages are four rigid links connected by four revolute joints and arranged into a closed chain. When the joints have their axes meeting at infinite, the linkage is called planar, and the links, if assumed to have zero thickness, move on a common plane, as shown in Fig. 1(a). Usually, links are bars and, given their cross shape of connected linkages, the derived structures are commonly known as scissor-like structures. When the joints have axes meeting at a real point, the linkage is called spherical because the outermost

points of the links, if assumed to have equal length, move on the surface of a sphere. Since the links are the portions of planes defined by the axes of the rigid joints, they are modelled as rigid plates. They are also known as origami-like patterns, and, if the sum of the planar angles meeting at a vertex is equal to 2π, they are strictly origami, as shown in Fig.1(b).

As the definitions may suggest, there are analogies between the two types of mechanisms. In both cases, links are free rigid bodies whose position is defined by three variables, which for planar linkages are the two translations and one rotation within a plane, and for spherical linkages are the rotations around three perpendicular axes. Therefore, their mobility formula is the same, and it returns one degree-of-freedom (DOF).

The dimensional compatibility and possible intersections between the links are disregarded from a kinematic perspective. The exact shape of the links is irrelevant; relevant is only how the joints constrain their reciprocal motion. Specifically, the revolute joints impose that the only admissible motions are rotations around their axes. Given the isometric motion of the rigid links, the rotatability range only depends upon the effective length of the link, which is the distance between the joints. Referring to Fig. 1(a), the effective length of one planar link is the linear distance a between the axes of its adjacent joints, while, in case of the spherical link, Fig. 1(b), the effective length is the arc length a between the axes, which, assuming a unit radius R of the containing sphere, reads $a = R \cdot \alpha = \alpha$. Hereinafter, when referring at once to both types of mechanisms, an uppercase latin letter may denote either the link or its length depending on the context.

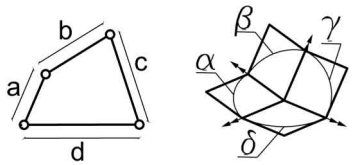

(a) (b)

Figure 1: a) A planar and b) a spherical $4R$-linkages.

Of interest for modular structures are linkages whose links are capable of reaching a coplanar position. Coplanar here refers to the extrusion of the links in between the axes of their end joints, so the definition applies to both types of mechanism. Working on deployable planar $4R$ bars, Escrig [16]

identified linkages that become coplanar as those that, given their ordered links having effective length a, b, c, d, fulfil

$$(a + b) = (c + d). \tag{1}$$

Such linkages rotate from a generic position to a deployed, overlapping position. Meanwhile, the Kawasaki–Justin theorem [20, 21] for folding of strict origami states that a one-vertex crease pattern folds flat if and only if the alternating sum and difference of the angles around the vertex add to zero:

$$\sum_{i=1}^{n} (-1)^{i-1} \alpha_i = 0. \tag{2}$$

In case of a $4R$ linkage, Eq. 2 reads

$$\begin{cases} \alpha + \beta + \gamma + \delta = 2\pi & \text{(3a)} \\ \alpha - \beta + \gamma - \delta = 0 & \text{(3b)} \end{cases}$$

When they are on a flat piece of paper, such linkages already lie all side by side in a plane and rotate to a stacked yet coplanar position. It is helpful to remark that the kinematic models do not address possible self-intersections. When physically constructing planar mechanisms, links are usually set on parallel planes, and the potential problem is disregarded. In spherical mechanisms, intersecting links would keep intersecting and crossing once constructed. The problem, firstly addressed by Maekawa, can be solved by assigning a compatible direction of folding to the links, or mountain-valley assignment. This is not an issue in linear assemblies of $4R$ linkages as the ones of interest here, while it can affect 2-way assemblies of links. The reader is referred to [22] for an extensive discussion.

Dealing with general spherical linkages, a cause of confusion is that the angle between two joints may be computed from any of the two ends of the joint's axes in the unit sphere. Chiang has developed an unambiguous approach by considering that the rotatability of a linkage is unchanged if any two angles larger than the right angle are substituted with their supplementary. Then, if the total number of links larger than the right angle is even, any two of those larger links can be switched to their supplementary; if the total number of links larger than the right angle is odd, the two largest ones are switched [14]. It should also be noted that no two adjacent angles should be equal to $\pi/2$, because, in such a situation, the two links would be in an

idle position. Being α any of the ordered set of links within the linkage, this reads $\alpha = \pi/2$, which implies

$$\gamma, \beta \neq \pi. \tag{4}$$

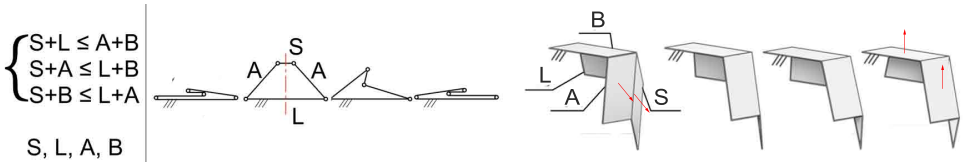

Figure 2: A Grashof linkage is characterized by special relationships among the effective length of its links, which allow at least one link to perform a full rotation.

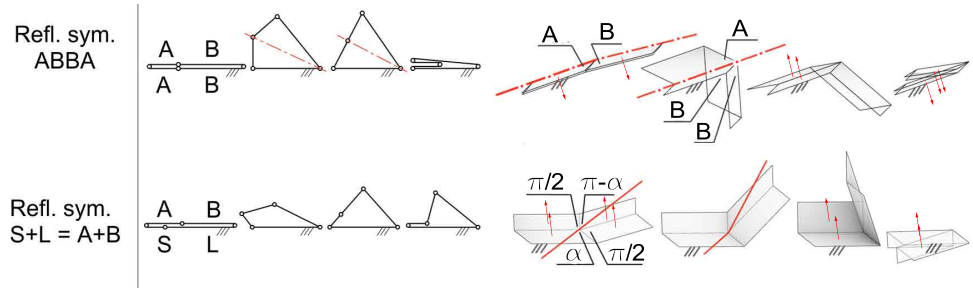

Figure 3: A linkage that reaches one stacked and one overlapping coplanar position is a Grashof linkage further characterized by a plane of reflective symmetry.

Given the simplification by Chiang, the Grashof's criterion for the rotatability of planar linkages can be extended to the spherical one without the need to obey Eq. 3a and as such allowing the design of non-"strict" origami. A Grashof linkage is one where the shortest link can perform a full rotation, which means that the linkage has at least two partially coplanar positions, Fig.2. Its conditions are

$$\begin{cases} S + L \leq A + B & \text{(5a)} \\ S + A \leq L + B & \text{(5b)} \\ S + B \leq L + A & \text{(5c)} \end{cases}$$

where S and L denote the shortest and the longest link respectively, and A, B denote the remaining links. If the equalities are verified, then larger coplanarities arise. In fact, it can be noted that Eq. 1 and Eq. 3b fulfil the equality in Eq. 5a.

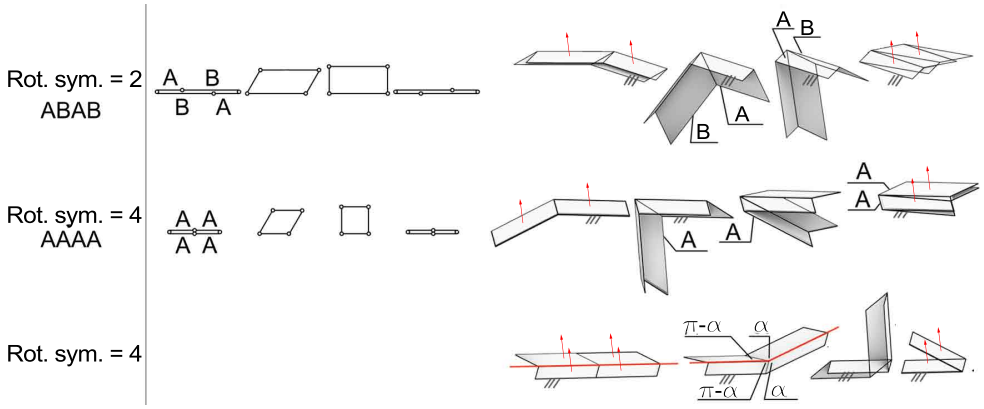

Figure 4: A Grashof linkage further characterized by a point of rotational symmetry of order 2 or 4 reaches two fully coplanar positions.

Building on this idea, it can be found where all links reach two coplanar states. If a reflection symmetry is further imposed on the linkage, Fig. 3, then two possibilities arise. The first and more general one is where all expressions in Eq. 5 are equalities: links in sequential order have length $ABBA$, with two joints on the symmetry plane. This is known in planar kinematics as a deltoid linkage. In one coplanar position, two links are re-entrant and surmounted by the other two. The spherical mechanism folds the same way. The second case holds when only the expression (5a) becomes an equality: the symmetry plane passes through the middle of the plates. In spherical linkages, the sequential links have necessarily length $\alpha, \pi/2, (\pi - \alpha)$, and $\pi/2$. This is the so called Barreto Mars folding [23], which, due to its two right angles, slips away from the simplifying assumptions of Chiang. If instead a rotational symmetry of at least degree two is imposed over a linkage satisfying Eq. (5), Fig. 4, the sequential links have lengths A, B, A, and B; they rotate from a stacked, coplanar position, to another stacked, coplanar position. In the origami case, this is obtained further imposing that no couple of joints can be in an idle state, which reads $\alpha+\beta \neq \pi$. As depicted in the figure, a symmetry of degree 4 means that all links have equal length, thus composing an $AAAA$ linkage. The origami allows a particularly compact bounding envelope in the fully folded configuration and it is known as Brunner [24], egg -box tiling [25] and perhaps under other names. Finally, below it is depicted the classical Miura Ori spherical linkage [6, 17, 26], whose links in sequential order have effective length α, $(\pi-\alpha)$, $(\pi-\alpha)$, and α. As by the simplification procedure

suggested by Chiang, its transmission angle is equal to the one of a linkage whose links are $\alpha, \alpha, \alpha, \alpha$, and such, as discussed in Section 2.3, it imposes low kinematic constraints on the motion of assemblies. Interestingly however, since its links sum up to 2π, in one coplanar position links lie side by side on a plane like a $ABBA$ planar linkage.

2.2. Notes on mechanics

In order to get a more complete vision of the motion and evaluate the role of the spatial arrangement of the joints, the deformation energy of the linkages has been analysed independently for each configuration. Figs.5(a) and 6(a) illustrate the linkages under investigation. In the pictures, the dark coloured plates are fixed, whereas external moments are applied to the linkages along the red coloured doubled arrow. To differentiate each stiffness contribution, due to the links and the joints, following the example in [27], each link is modelled as a frame of sides with unit-length (in m) and stiffened by double diagonals. With reference to Figs. 5(b) and 6(b), each element of the frame is modelled as a beam with circular cross-section (10^{-1}m in diameter). The torsional stiffness ratio between the four joints and the remaining link elements has been set to 10^{-1}, with the torsional rigidity of the joints given by the shear modulus $G_j = 10^8$kPa, whereas the other elements equating to $G_l = 10^9$kPa. The imposed moment is $M = 10$kNm. As can be seen in Fig.s 5(a) and 6(a), the deformation energy of the linkages has been computed for different motion stages, starting from an configuration where the dihedral angle between the fixed link and its rear link is zero, and expanding such angle at intervals of 30° until the entire range of motion of the linkage is depicted. The deformation energy, Figs.5(c) and 6(c), is computed independently for each configuration as the change of the internal elastic energy from an unloaded to the loaded case, and measures the scalar product of the external nodal loads and nodal displacements. For any given action, the geometrical parameters affecting the deformation of the planar linkages are the length of the links and their inclination versus the reaction provided by the ground link. The planar linkage behaves like a semi-rigid portal frame subjected to a moment. Toward the mid-way configuration, the links are mainly subjected to bending action, with linkage $ABAB$ deforming more than the otherwise equal linkage $AAAA$ due to its longer links; when the links are in a configuration closer to the stacked position, the shear force becomes significant, and the deformation increases accordingly, Fig.5(c). Eventually,

when all links are perfectly coplanar, the linkage behaves like a cantilever, which is read by the peak in the deformation energy.

The geometrical parameters affecting the deformation of the spherical linkages are the dihedral angle between the links and their planar angle at the common vertex, [28], which makes their evaluation less intuitive. However, as in the planar linkage, when two links are coplanar and stacked, they tend to act together. In general, the linkage may again behave like a cantilever, as in the final configurations of linkages $AAAA$ and $ABAB$, or both the end configurations of the Miura linkage, Fig. 6(a). However, suppose the moment action is aligned with an edge of the stacked fixed link. The deformation energy reaches the minimum, as in the initial configuration of the the $AAAA$ and $ABAB$ linkages.

Comparing the plots depicted in Fig. 5(c) and 6(c), the planar linkages generally exhibit higher compliance than the spherical ones. The latter are are non-developable assemblies (the Miura being the exception), i.e. intrinsically unable to have their links lying down adjacent to each other in a plane without stretching. However, it shall be remarked that the dimensions of the links have been chosen arbitrarily. These decisions affect in a non-linear manner the values of the deformation energy.

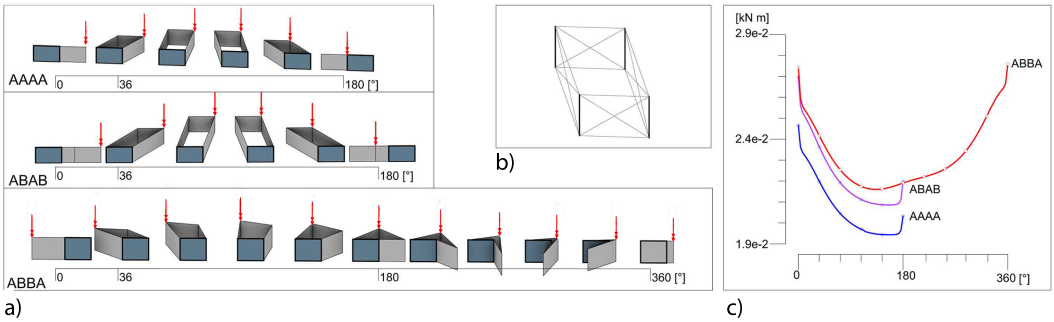

Figure 5: a) Planar $4R$-linkages configurations, b) structural model for the analysis and c) energy graph.

2.3. The assembly constraints

When assembling linkages one to another, mobility is equal to one if and only if each added linkage shares at least two links with the others [29]. Between two planar linkages, the shared links are obtained by elongating them; sometimes, the links are further kinked to create angulated bars [30,

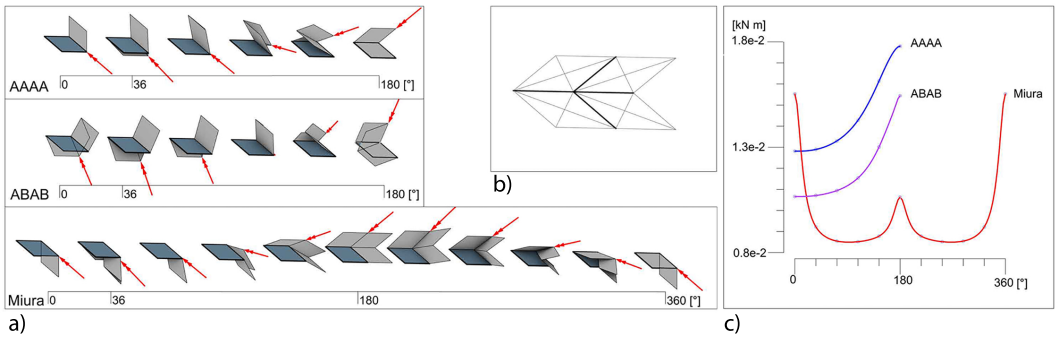

Figure 6: a) Spherical $4R$-linkages configurations, b) structural model for the analysis and c) energy graph.

31]; alternatively, the second part of the shared link is partially overlapping with the first part [32]. In spherical linkages, quadrangular plates are by far the most common choice because each of their vertexes, being degree-4, can be the centre of a $4R$-linkage.

The input and output transmission angles must be the same throughout to guarantee that all linkages reach the coplanar states. A differential rotation between two shared links would not be possible because a 1-DOF revolute joint connects them. The value of these angles at any motion stage depends on the reciprocal length of the links within the overall assembly and ensuring a uniform motion is generally a non-trivial subject [33, 34]. If the analysis is limited to fully rotatable linkages as the ones of interest here, however, the symmetry operations previously discussed ensure that the transmission angle is constant throughout at any rotation stage and independent of the exact effective length of the links.

In Fig. 7, the previous linkages are depicted and their possible input θ_i, τ_i, and output θ_{i+1}, τ_{i+1} transmission angles are indicated. Considering linkages with rotational symmetry, Fig. 7(a), the parallelism between links imposes that both angles τi and θi are constant in i. Other fully rotatable linkages can be added in any direction regardless of their effective lengths. Meanwhile, in linkages with reflection symmetry, Fig. 7(b), just the angle that lies within the orbifold, τ in the figure, is constant. Just in that direction, linkages can be freely added. On the contrary, the relationship between angles θ_i and θ_{i+1} depends on the exact proportion of the effective length of the links. Thus, if the transmission angle is θ_i, then a uniform motion is possible only if the very same linkage, or a scaled version of it, is added. This

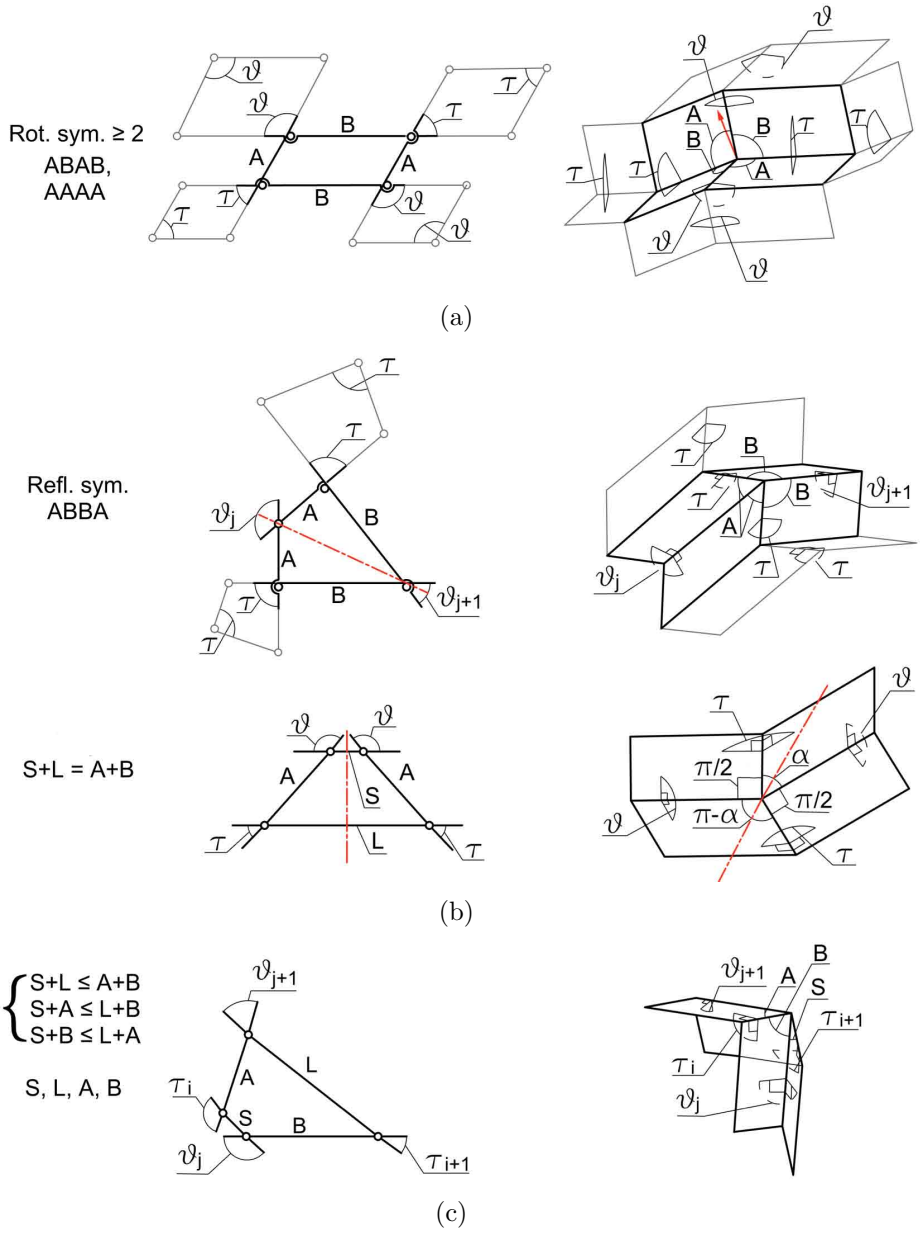

Figure 7: Transmission angles between linkages. a) Linkages with rotational symmetry have two directions of constant transmission angle regardless the effective length of the links. b) In linkages with reflective symmetry, the transmission angle lying within the orbifold is constant throughout the assembly regardless of the effective length of the links. c) In an assembly of generic Grashof's linkages, the input and output angles change linkage by linkage.

last condition also applies to the other linkages where the input and output transmission angles differ from each other, Fig. 7(c). Finally, a compelling case is the one where the symmetry plane passes through the links, lower case of Fig. 7(b): here, despite the transmission angles are constant, the underlying symmetry constrains the specific length of the links, and such again only equal or uniformly scaled linkages can be added. These conditions are sufficient to ensure that the overall assembly rotates in a uniform way and reaches a fully coplanar state.

3. Interpolation of spatial open curves

By applying the relevant constraints to the kinematic models described in Section 2.1, it is possible to create fully rotatable assemblies. Here, algorithms for interpolating spatial open curves through such assemblies are presented with $ABBA$ and $ABABA$ linkages. As mentioned in Section 1, it should be remarked that the following routines are not the only possible ways to interpolate a curve; beside, they can also be combined. However, alternative procedures often require locally switching between the types of linkage, or they do not allow setting the interpolation points a priori. In the following algorithms, the symmetry operations characteristic of the linkage are extended to the assembly procedures, and such the mechanism results fully rotatable regardless the specificity of the curve.

3.1. Linkages with reflection symmetry

A first computational approach accounts for the curvature of the target geometry, and produces assemblies of $ABBA$ and/or $AAAA$ linkages. As a reflection symmetry characterises the linkage, so more linkages are connected through such an operation. Consider the piecewise continuous curve $C : R \rightarrow R^3$ depicted in Fig.8 and evaluate the curve at desired discrete values s_i, i from 1 to m, where $C : s_i \mapsto P_i$. Linearly interpolate the resulting points and trace the osculating planes $\mathcal{OP}_i$, spanned by $\{\mathbf{t_i},\mathbf{n_i}\}$, at midpoint to the segments $\overline{\mathrm{P_{i-1}P_i}}$. Any binormal plane $\mathcal{BP}_i$, spanned by $\{\mathbf{b_i},\mathbf{n_i}\}$, is a plane of reflection symmetry that maps P_{i-1} to P_i.

The design of the linkages can now be initiated. Dealing with the planar case, Fig. 9, consider two consecutive points P_i and P_{i+1} and trace from each of them two lines lying on $\mathcal{OP}_{i+1}$, and being at an angle to each other equal to the desired transmission angle τ. The lines intersect along $\mathbf{n_{i+1}}$. The intersection points M_i, L_i, together with P_i and P_{i+1}, are the vertexes of the

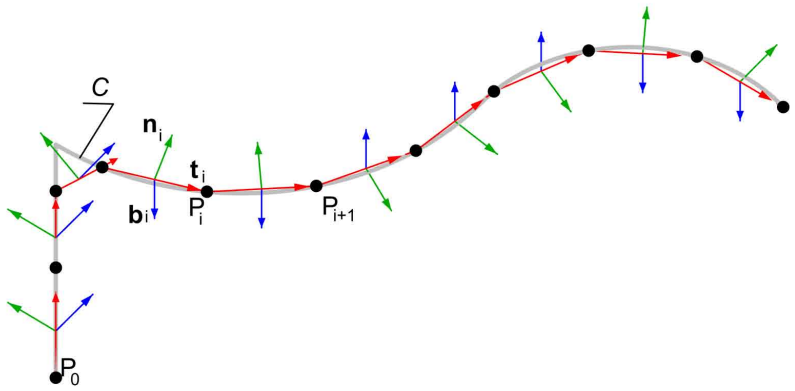

Figure 8: The reference curve C, its linear interpolation points and the local curvature frames at the midpoints of the resulting segments

linkage. The other linkages are found by construction. The linkage just made must share with the following linkage its two outer links, which can thus be extended up to $\mathcal{BP}_{i+2}$ centered at midpoint of the segment $\overline{\mathrm{P_{i+1}P_{i+2}}}$. The intersection points of these lines with the plane are the mid vertexes M_{i+1}, L_{i+1} of linkage spanning $\overline{\mathrm{P_{i+1}P_{i+2}}}$. The remaining two links are obtained by mirroring around $\mathcal{BP}_{i+1}$. The procedure is propagated to the rest of the curve, Fig. 9.

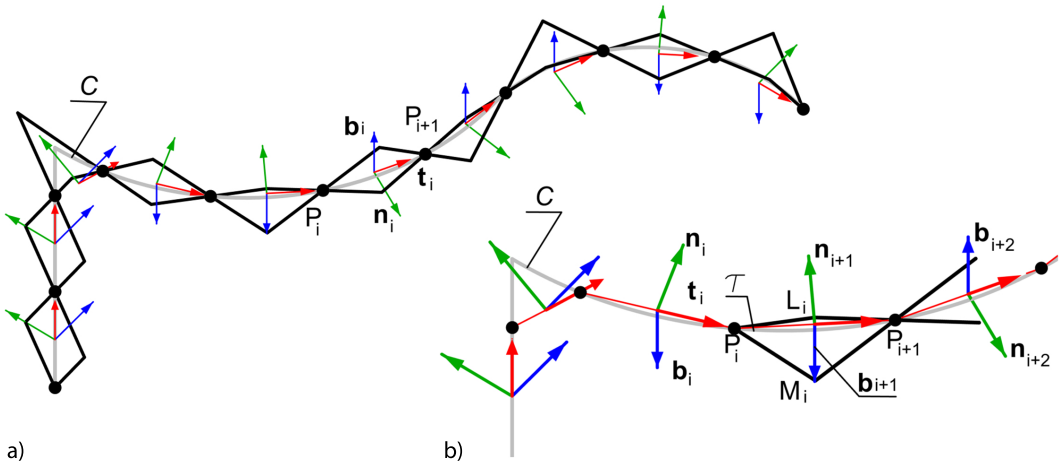

Figure 9: a) The assembly of planar $ABBA$ linkages superimposed over the reference curve C. b) Initial steps of the interpolation process

The procedure for spherical linkages is described with reference to Fig. 10(a). On $\mathcal{OP}_i$, trace a line $l_{1,i}$ through P_i. Translate $l_{1,i}$ along $\mathbf{n_i}$, setting line $l_{2,i}$. Rotate the latter along the former by the desired transmission angle τ. Shatter the three lines at $\mathcal{BP}_{i+1}$ and $\mathcal{BP}_i$. The resulting mid segments are the longitudinal edges of the first two plates. By connecting their corresponding vertexes, the plates are completed. Mirror the 3 lines around plane $\mathcal{BP}_i$, shattering them at $\mathcal{BP}_{i+1}$. The segments comprised between the planes are the longitudinal edges of the remaining plates, which can be completed as before. Notice that, if $\mathbf{t_i} = \mathbf{t_{i+1}}$, if the curve is straight up to the next segment, then it should be imposed that $l_{1,i} \nparallel \mathbf{t_i}$, Fig. 10(b). This condition fulfils the inequality in Eq. 4 by ensuring that α_i, $\beta_i \neq n\pi/2$, which would reduce the spherical mechanism to a concertina one. The successive linkages are found repeating the mirroring and shuttering processes, Fig. 11.

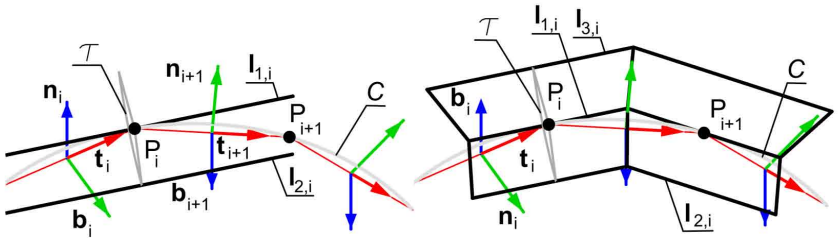

(a)

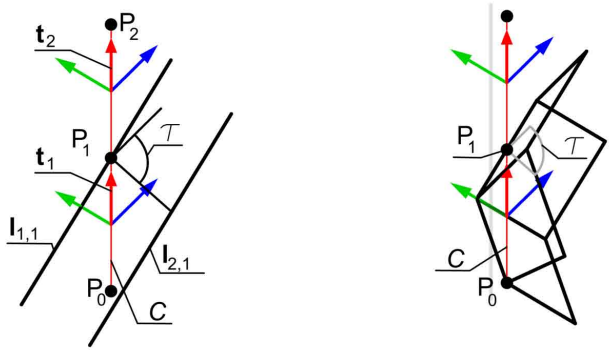

(b)

Figure 10: a) Interpolating a curve through an assembly of spherical $ABBA$ linkages. b) If the first two points used for the design of the assembly are cotangent, it should be avoided to set the longitudinal edge $l_{1,i}$ of the first plate along the direction vector $\hat{\boldsymbol{t}}_{\boldsymbol{i}} = \hat{\boldsymbol{t}}_{\boldsymbol{i+1}}$.

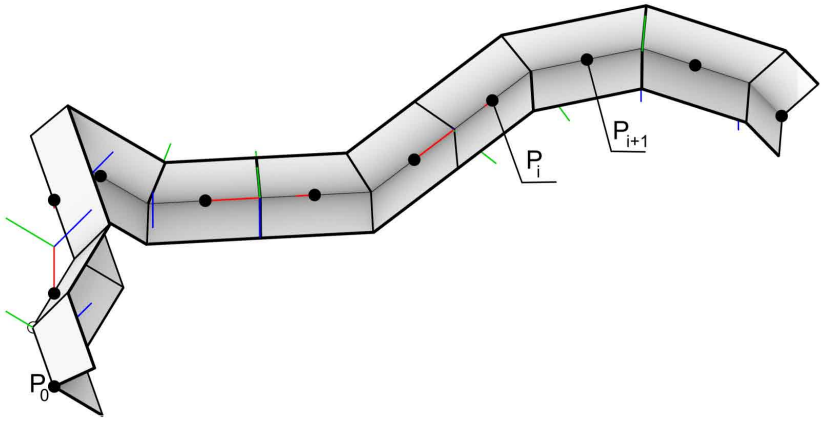

Figure 11: A spherical assembly of $ABBA$ linkages superimposed over the reference curve.

These assemblies are fully rotatable because the symmetry axes guarantee that the transmission angle is constant. It can be noted that, even when the first linkage is an $AAAA$ type, the successive ones will change to $ABBA$ by construction as soon as the segments approximating the curve are at an angle to each other. The linkages $ABBA$ will point toward the local centre of curvature, and such design procedures that involve $ABBA$ linkages have been called polar in [35, 36], and in [37], concerning respectively planar and spherical linkages.

3.2. Linkages with rotational symmetry

The following algorithms are derived from the procedure described in [38], which they substantially extend from the degenerate case of $AAAA$ spherical linkages [38] to all linkages with rotational symmetry ($ABAB$ and $AAAA$ linkages), either spherical or planar. They lead to fully rotatable assemblies where joints whose axes share a plane at a rotation stage keep sharing a plane throughout the motion. Before proceeding, it is worth noting that coplanar joints are an intrinsic characteristic of $ABAB$ linkages, see Fig. 7(a), but the feature is lost in current alternative assembling procedures for spatial figures. Dealing with planar linkages, Fig. 12, on a plane containing points P_i and P_{i+1}, trace from P_i two vectors $\mathbf{a}$, $\mathbf{b}$ at an angle τ equal to the desired transmission angle. The proportion $\|\mathbf{a}\|/\|\mathbf{b}\|$ between the lengths of these vectors will be the proportion between the length of the links within all the i, j linkages spanning between any two consecutive P_i, P_{i+1} points:

$$\begin{aligned} \|\mathbf{a_{i,j}}\| &= k_{i,j}\|\mathbf{a}\| = \forall \mathbf{i}, \mathbf{j} \\ \|\mathbf{b_{i,j}}\| &= k_{i,j}\|\mathbf{b}\| = \forall \mathbf{i}, \mathbf{j}. \end{aligned} \tag{6}$$

Accordingly, setting $\mathbf{a}/\mathbf{b}$ =1 will lead to $AAAA$ linkages, while $\mathbf{a}/\mathbf{b} \neq 1$ will lead to $ABAB$ ones. Connect the tips of $\mathbf{a}$, $\mathbf{b}$, and bisect the resulting segment with a line passing through P_i. Call respectively $\hat{\boldsymbol{l}}$ and $\hat{\boldsymbol{m}}$ the direction vectors of these lines. These will be the directions of the diagonals of the linkage. Type $ABAB$ linkages subjected to uniform scaling, Fig. 12(a), and / or translation, Fig. 12(b), create similar triangles whose diagonals stay parallel, which guarantee that the axes of the joints are parallel too during motion. From P_{i+1}, trace a line with direction $\hat{\boldsymbol{l}}$ and intersect it with a line passing through P_i with direction $\hat{\boldsymbol{m}}$. From the intersection point X_i, traces lines along directions $\hat{\boldsymbol{a}}$ and $\hat{\boldsymbol{b}}$. Intersect them with lines again along direction $\hat{\boldsymbol{a}}$ and $\hat{\boldsymbol{b}}$ through P_i and with the equally oriented lines through P_{i+1}. The intersection points are the missing vertexes of two linkages spanning between points P_i and P_{i+1}. By construction, the linkages are uniformly scaled and with the same transmission angle. In order to complete the assembly, the process can be repeated, provided as usual with planar linkages that linkages are reoriented in different planes when necessary. To accommodate a rotation between P_{i+1} and P_{i+2} while ensuring that the joints' axes stay parallel, it is sufficient to rotate the two links of linkages i closer to P_{i+1} around the axis $\hat{\boldsymbol{l}}$ centred at P_{i+1}, up to the plane passing through the rotation axis and the segment $\overline{\mathrm{P_{i+1}P_{i+2}}}$, Fig. 12(e). Then, point X_{i+1} can be found as before and the new linkages completed. The presented procedure however may lead to some links moving independently. Therefore, a secondary routine, which can be nested in the algorithm, should verify that every link not at the end of the assembly is shared by two linkages and add a new one otherwise. The two linkages to the right in Fig. 12(c) partially lie on different planes, but they share two links. The ones illustrated in Fig. 12(d) shared just one link, and another one was added. The whole assembly is depicted in Fig. 13.

The procedure for spherical linkages also involves the usage of coplanar joints that stay coplanar throughout the assembly and at any folding stage. In the case of $AAAA$ linkages, transversal and longitudinal joints will be on two families of perpendicular planes. In the case of $ABAB$ linkages the two planes will be at an angle $\neq n\pi/2$. With reference to Fig.14(a), call $\mathbf{a}$ the vector from point P_i to point P_{i+1}. Set a plane Σ perpendicular to it and centred at P_i. On the plane, set two vectors $\mathbf{c}'$ and $\mathbf{d}'$ subtending the desired

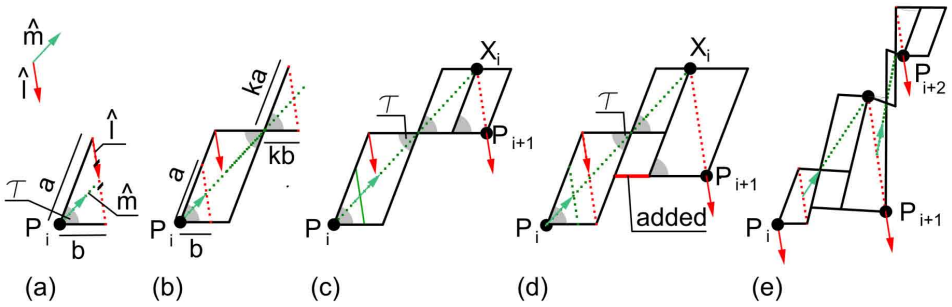

Figure 12: a) Uniformly scaled $ABAB$ linkages guarantee that the axes of the joints are parallel too during motion. b) The propriety is preserved up to the translation of the linkage. c) Each internal link should be shared by two linkages, and (d) a link should be added otherwise. e) The linkages can have parallel joints also if lying on different planes rotated to each other along vector $\hat{\boldsymbol{\imath}}$.

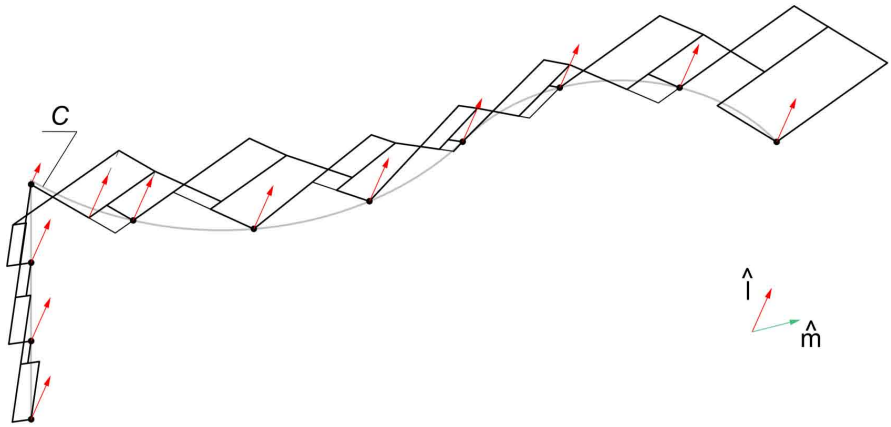

Figure 13: A linear assembly of $ABAB$ linkages superimposed over the reference curve C.

transmission angle τ and call $\boldsymbol{s}$ their bisector, Fig.14(b). If generic $ABAB$ linkages are desired, Fig.14(c), rotate Σ around a vector $\boldsymbol{x}$ lying on it and passing through P_i, ensuring that $\boldsymbol{x} \times \boldsymbol{s} = 0$, $\boldsymbol{x} \cdot \boldsymbol{s} = 0$. Call Ξ the resulting plane. Project $\mathbf{c}'$ and $\mathbf{d}'$ on Ξ along $\hat{\boldsymbol{a}}$, Fig.14(d). The projected segments $\mathbf{c}$ and $\mathbf{d}$ are the transversal edges of the first two plates, and their direction, in alternate order, is the direction of the transversal edges of all the plates within the assembly. Finally, find the bisector of $\hat{\boldsymbol{c}}$ and $\hat{\boldsymbol{d}}$ emanating from P_i, and rotate $\mathbf{a}$ around it by a planar angle, finding vector $\mathbf{b}$, Fig.14(e). The directions $\hat{\boldsymbol{a}}$ and $\hat{\boldsymbol{b}}$ are, in alternate order, the directions of the longitudinal edges of all the plates within the assembly. To complete the first two plates, it is sufficient to translate $\mathbf{c}$ and $\mathbf{d}$ from P_i to P_{i+1} and connect their endpoints longitudinally along $\hat{\boldsymbol{a}}$, Fig. 14(e). If $AAAA$ linkages are desired, the procedure is illustrated in Fig.15, and differs only because it should be $\hat{\boldsymbol{x}} \times \hat{\boldsymbol{s}} = 0$, Fig.15(c). In both scenarios, the rotation satisfies the inequality in Eq. 4 by ensuring that the plates have planar angles different from $n\pi/2$. To complete the linkage, Fig. 16(a), set a plane $\hat{\boldsymbol{c}}\hat{\boldsymbol{d}}$ centred in P_{i+2}. Intersect it with a line along $\hat{\boldsymbol{b}}$ passing through P_{i+1}, so finding point P'_{i+2}. From this and from P_{i+2}, trace lines both along directions $\hat{\boldsymbol{a}}$ and $\hat{\boldsymbol{b}}$, finding their two intersections. Connect the four points (anti)clockwise, obtaining 4 segments. Of these, enumerated starting from P_{i+2}, delete either the first two or the last two segments at choice, as they are the traces of redundant plates. The remaining segments are the transversal edges of the missing plates. To complete the plates, extrude the segments along direction $\hat{\boldsymbol{b}}$, from P_{i+2} to P_{i+1}. Successive linkages can be created in the same way. As with the planar case, the algorithm further contains a mobility check to ensure that no plates can rotate independently. This means that at each internal vertex four plates should meet, and that a possible missing plate should be added otherwise. Since the plates in this design procedure are parallelograms, the edges of the missing plates are obtained simply translating the edges of the adjacent ones, as illustrated in Fig. 16(b). The whole assembly is depicted in Fig. 17.

The transmission angle is constant and coplanar joints' axes stay coplanar throughout the motion. The alternative procedures for interpolating spatial figures that have been developed elsewhere employ $ABAB$ linkages that are not uniformly scaled throughout the assembly, making the twisting angle variable in time. Such algorithms, presented in [38] dealing with $AAAA$ spherical linkages and in [35, 39] concerning $ABAB$ planar ones, are shorter than the ones presented here and tend to employ fewer links. In this paper,

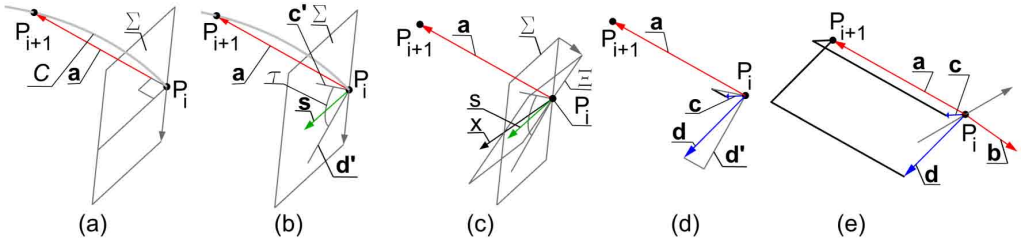

Figure 14: Procedure for constructing $ABAB$ linkages. Setting a longitudinal edge vector $\hat{\boldsymbol{a}}$ (a); setting the transmission angle τ (b); finding the transversal edge vectors $\hat{\boldsymbol{c}}$, $\hat{\boldsymbol{d}}$ (c); applying a rotation symmetry to find the second longitudinal vector $\hat{\boldsymbol{b}}$ (d); finalising the design of the first plates (e).

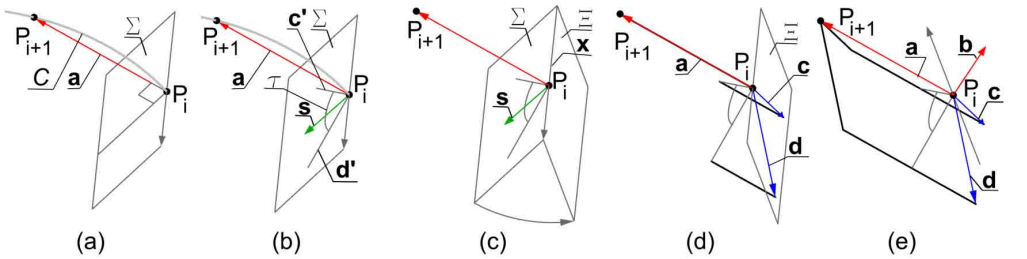

Figure 15: The procedure described in Fig. 14 modified to generate $AAAA$ linkages.

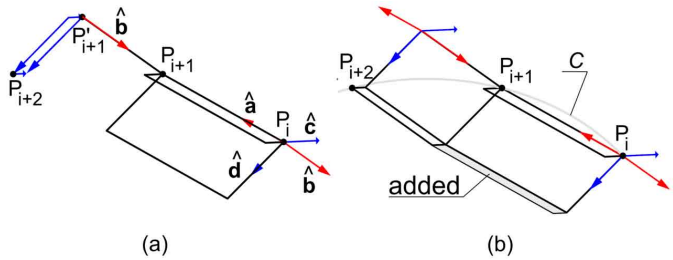

Figure 16: Procedure for constructing an assembly of parallel $ABAB$ linkages. a) Finding the trace of given plates on parallel planes. b) Completing the linkage.

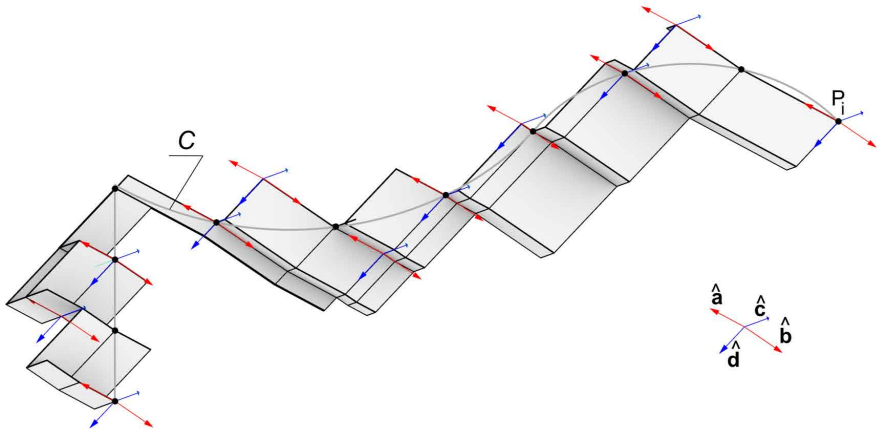

Figure 17: A linear assembly of $ABAB$ linkages superimposed over the reference curve C.

the intent is to highlight the characteristics of the linkages. It has been preferred to maintain consistently parallel axes whether linkages lie in a plane or $3D$. Moreover, as addressed in [38, 39], the twisting strongly limits the possibilities to create closed curves, tessellations, and surfaces. Therefore, the presented algorithms may broaden the design space of assemblies of $4R$-linkages.

4. Conclusions

This research has presented a unifying approach for the kinematic synthesis of modular spherical and planar assemblies of $4R$-linkages. These linkages are the simplest and most employed ones, but shared investigations on their modular assemblies have been lacking so far. Building on the classical Grashof's criterion for the rotatability of planar $4R$-linkages, linkages have been classified based on their capability to reach a coplanar state. The classification method relies only on the proportion between the effective length of the links, which is meant here as distance between the axes of the joints. Linkages that can rotate between two coplanar states possess rotational or translational symmetries. Since such a large rotatability range is considered a critical performance when employing kinetic modular structures, the focus has been made on them and related algorithms for interpolating spatial curves through a prescribed set of points have been described. The procedures presented are not the only possible ones for approximating target figures. Because the algorithms maintain the kinematic model invariant within

the assembly, their applicability is not limited to a certain curve or family of curves. For example, algorithms for producing $ABAB$ or $AAAA$ linkages that twist neither when organised along a planar figure nor in space have been developed. As for the mechanics, our findings shall not be intended to decide which type of linkages are stiffer for a given load but only to qualitatively acknowledge similarities in the mechanics of symmetrical planar and spherical linkages. This work has not covered surfaces and closed curves. In such cases, it is necessary to consider both the longitudinal and transversal transmission angles and to consider dimensional constraints to maintain the loop of closed links in time. However, the kinematic model and assembly constraints will stay valid, and as such, they can be considered a shared model that can withstand further extension. Given that planar linkages' kinematic and mechanical behaviour is easier to understand intuitively, by setting an analogy between these and the spherical linkages, this research also aimed to favour a deeper understanding of the behaviour of simple origami structures, which can be helpful in the highly interdisciplinary conceptual design space of origami-inspired structures.

References

[1] F. ESCRIG, P. Varcárcel, La obra arquitectónica de emilio pérez piñero, Boletín Académico de la ETSA (16) (1992) 3–4.

[2] C. J. Gantes, Deployable structures: analysis and design, Wit Press, 2001.

[3] F. E. Pallares, Modular, Ligero, Transformable: Un paseo por la arquitectura ligera móvi, Editorial Universidad de Sevilla-Secretariado de Publicaciones, 2012.

[4] B. R. Russell, A. P. Thrall, Portable and rapidly deployable bridges: Historical perspective and recent technology developments, Journal of Bridge Engineering 18 (10) (2013) 1074–1085.

[5] S. Pellegrino, Deployable structures, Vol. 412, Springer, 2014.

[6] K. Miura, Method of packaging and deployment of large membranes in space, The Institute of Space and Astronautical Science report 618 (1985) 1–9.

[7] H. Huzita, Proceedings of the First International Meeting of Origami Science and Technology: Ferrara, Italy, December 6-7, 1989 Casa Di Lodovico Ariosto, Universita, 1990.

[8] M. B. Robert J. Lang, Z. You, The Proceedings from the Seventh Meeting of Origami, Science, Mathematics and Education, Tarquin Pubns, 2018.

[9] M. Meloni, J. Cai, Q. Zhang, D. Sang-Hoon Lee, M. Li, R. Ma, T. E. Parashkevov, J. Feng, Engineering origami: A comprehensive review of recent applications, design methods, and tools, Advanced Science 8 (13) (2021) 2000636.

[10] D. Rus, M. T. Tolley, Design, fabrication and control of origami robots, Nature Reviews Materials 3 (6) (2018) 101–112.

[11] J.-H. Cho, M. D. Keung, N. Verellen, L. Lagae, V. Moshchalkov, P. Van Dorpe, D. H. Gracias, Nanoscale origami for 3d optics, Small 7 (14) (2011) 1943–1948.

[12] C. H. Chiang, Design of spherical and planar crank-rockers and double-rockers as function generators—i, Mechanism and machine theory 21 (4) (1986) 287–296.

[13] C. H. Chiang, Spherical kinematics in contrast to planar kinematics, Mechanism and Machine Theory 3 (27) (1992) 243–250.

[14] C. H. Chiang, On the classification of spherical four-bar linkages, Mechanism and Machine Theory 19 (3) (1984) 283–287.

[15] A. P. Murray, P. Larochelle, A classification scheme for planar 4r, spherical 4r, and spatial rccc linkages to facilitate computer animation, ASME Paper No. DETC98/MECH-5887 10 (1998).

[16] F. E. Pallares, Expandable space structures, International Journal of Space Structures 1 (2) (1985) 79–91. doi:10.1177/026635118500100203.

[17] T. Tachi, Generalization of rigid-foldable quadrilateral-mesh origami, Journal of the International Association for Shell and Spatial Structures 50 (3) (2009) 173–179.

[18] A. E. Yıldız, Mobile structures of santiago calatrava : other ways of producing architecture, Master's thesis, Middle East Technical University (2007).

[19] F. Maden, K. Korkmaz, Y. Akgün, A review of planar scissor structural mechanisms: geometric principles and design methods, Architectural Science Review 54 (3) (2011) 246–257.

[20] On the relation between mountain-creases and valley-creases of a flat origami.

[21] D. Huffman, Curvature and creases: A primer on paper, IEEE Transactions on Computers 25 (10) (1976) 1010–1019. doi:10.1109/TC.1976.1674542.

[22] R. J. Lang, Twists, tilings, and tessellations: mathematical methods for geometric origami, CRC Press, 2017.

[23] P. T. Barreto, Lines meeting on a surface: The "mars" paperfolding, in: K. Miura (Ed.), Origami science and art. Proc. Origami II, 1994, Seian University of Art and Design, 1997, pp. 343–359.
URL https://books.google.dk/books?id=7gjengEACAAJ

[24] A. Brunner, Expansible surface structures, U.S. Patent No. 3,362,118 (7 1965).

[25] R. Xie, Y. Chen, J. M. Gattas, Parametrisation and application of cube and eggbox-type folded geometries, Int. J. Space Structures 30 (2) (2015) 99–110. doi:10.1260/0266-3511.30.2.99.
URL https://doi.org/10.1260/0266-3511.30.2.99

[26] J. M. Gattas, W. Wu, Z. You, Miura-base rigid origami: Parameterizations of first-level derivative and piecewise geometries, Journal of Mechanical Design 135 (11), 111011 (10 2013). arXiv:https://asmedigitalcollection.asme.org/mechanicaldesign/article-pdf/135/11/111011/6223980/md_135_11_111011.pdf, doi:10.1115/1.4025380.
URL https://doi.org/10.1115/1.4025380

[27] E. Filipov, K. Liu, T. Tachi, M. Schenk, G. H. Paulino, Bar and hinge models for scalable analysis of origami, International Journal of Solids and Structures 124 (2017) 26–45.

[28] K. Liu, L. S. Novelino, P. Gardoni, G. H. Paulino, Big influence of small random imperfections in origami-based metamaterials, Proceedings of the Royal Society A 476 (2241) (2020) 20200236.

[29] V. Beatini, K. Korkmaz, Shapes of miura mesh mechanism with mobility one, International Journal of Space Structures 28 (2) (2013) 101–114. arXiv:https://doi.org/10.1260/0266-3511.28.2.101, doi:10.1260/0266-3511.28.2.101.
URL https://doi.org/10.1260/0266-3511.28.2.101

[30] C. Hoberman, Reversibly expandable doubly-curved truss structure, US Patent 4,942,700 (1990).

[31] Z. You, S. Pellegrino, Foldable bar structures, International Journal of Solids and Structures 34 (15) (1997) 1825 – 1847. doi:https://doi.org/10.1016/S0020-7683(96)00125-4.
URL http://www.sciencedirect.com/science/article/pii/S0020768396001254

[32] S. Bouten, Transformable structures andtheir architectural applications, Master's thesis, University of Ghent, Ghent (2015).

[33] N. Watanabe, K.-i. Kawaguchi, The method for judging rigid foldability, Origami 4 (2009) 165–174.

[34] T. Tachi, Simulation of rigid origami, in: R. Lang (Ed.), Fourth Int. Conf. Origami in Science, Mathematics, and Education (4OSME), A K Peters/CRC Press, New York, 2009, pp. 175–187. doi:A K Peters/CRC Press.

[35] F. Albermani, T. Langbecker, Kinematic and nonlinear analysis of foldable lattice structures, in: Structural Stability And Dynamics: With CD-ROM (Volume 1), World Scientific, 2003, pp. 653–659.

[36] K. Roovers, N. De Temmerman, Geometric design of deployable scissor grids consisting of generalized polar units, Journal of the International Association for shell and spatial structures 58 (3) (2017) 227–238.

[37] V. Beatini, Polar method to design foldable plate structures, Journal of the International Association for Shell and Spatial Structures 56 (2) (2015) 125–136. doi:10.1260/0266-3511.30.2.85.

[38] V. Beatini, Translational method for designing folded plate structures, International Journal of Space Structures 30 (2) (2015) 85–97. arXiv:https://doi.org/10.1260/0266-3511.30.2.85, doi:10.1260/0266-3511.30.2.85.
URL https://doi.org/10.1260/0266-3511.30.2.85

[39] K. Roovers, N. D. Temmerman, Deployable scissor grids consisting of translational units, International Journal of Solids and Structures 121 (2017) 45 – 61. doi:https://doi.org/10.1016/j.ijsolstr.2017.05.015.
URL http://www.sciencedirect.com/science/article/pii/S0020768317302184